NASA
Technical Memorandum 79237

AVRADCOM
Technical Report 79-38

EFFECT OF STEADY-STATE TEMPERATURE DISTORTION AND COMBINED DISTORTION ON INLET FLOW TO A TURBOFAN ENGINE

Ronald H. Soeder
Lewis Research Center

and

George A. Bobula
Propulsion Laboratory
AVRADCOM Research and Technology Laboratories
Lewis Research Center
Cleveland, Ohio

August 1979

SUMMARY

The results of an investigation to determine the effect of steady-state temperature distortion and combined steady-state pressure-temperature distortion on flow at the inlet to a turbofan engine are reported herein. Flow angle, static pressure, total temperature and total pressure instrumentation was placed between a rotatable hydrogen-fueled burner, rotatable-screen assembly and the engine inlet guide vanes. For all of the configurations, measurements were recorded at each of twelve, 30° steps of distortion rotation. Experiments were conducted with low-rotor speeds of 6000 and 8600 rpm and a Reynolds Number Index of 0.5. These parameters were based on the undistorted sectors at the engine inlet.

At the entrance to the engine, yaw angle (circumferential) was larger than pitch angle (radial). Both pitch and yaw angles were largest in the hub region of the engine inlet. As the flow approached the engine the yaw angle increased while the pitch angle decreased. Low-rotor speed only slightly effected pitch and yaw angle magnitude. A change in distortion extent produced a circumferential shift in the pitch and yaw angle variation but the flow angle amplitudes remained constant.

Along the inlet-duct and extended bullet nose walls the magnitude of the static pressure distortion increased exponentially as the flow approached the engine inlet. For the steady-state temperature distortion tests, static pressure variation along the inlet duct wall was a function of low-rotor speed and distortion extent.

INTRODUCTION

Recently, analytical effort has been directed towards evolving compressor models that can predict the effects of inlet distortion on the operating characteristics and performance of turbofan engines (ref. 1, 2 and 3). In the evaluation of these models, it is important to know the actual flow field at the face of an engine being subjected to upstream pressure, temperature or combined pressure and temperature distortions. Experimental investigations, therefore, have been conducted to determine the inlet flow distributions associated with various types of distortion. Flow distributions resulting from 180°-extent pressure distortion are reported in references 4, 5 and 6 and the effects of temperature distortions of 90° to 360° in extent are presented in references 7, 8 and 9.

The purpose of the investigation presented in this paper was to further evaluate inlet flow distributions due to temperature distortions of various extents and, also, inlet flow distributions resulting from combined pressure and temperature distortions. For this purpose, in addition to standard surveys of total pressure and total temperature at

the engine inlet, freestream flow angles were measured in radial surveys at two axial locations including the engine inlet guide vanes. Static pressures were measured along the inlet duct and extended bullet nose walls. In reference 10 static-pressure distortion amplification is discussed and predicted to be exponential upstream of the engine inlet. Lastly, total pressure and total temperature measurements were recorded at several axial locations between distortion devices (hydrogen burner and rotating-screen assembly) and the engine inlet.

Data are presented for two low-rotor speeds of 6000 and 8600 rpm and for a Reynolds Number Index of 0.5 (based on the undistorted sectors at the engine inlet). The data cover distortion extents of 90° to 180° for temperature distortion experiments and extents of 180° each for combined pressure and temperature distortion experiments.

APPARATUS

Engine

The engine used for this investigation was a production TF30-P-3 twin-spool turbofan engine. The engine has fixed inlet guide vanes (IGV's), 7th and 12th stage compressor bleeds and a variable exhaust nozzle. The engine was installed in an altitude chamber by a direct-connect type of installation as shown in figure 1. An engine schematic and instrumentation stations between the distortion generator and engine inlet guide vanes are shown in figure 2.

Distortion Devices

The gaseous-hydrogen-fueled burner used to produce steady-state temperature distortion was installed upstream of the engine inlet bellmouth (figs. 2 and 3). The burner had the capability of being rotated ±30° from the center position and was divided into four individually controlled quadrants. Air passing through the burner was heated in selected 90° sectors. Each 90° sector of the burner contained five swirl-can pilot burners to provide the ignition source for the hydrogen. In addition each 90° sector contained five annular gutters supported by one radial gutter and five-circular-tube manifolds (one inside each annular gutter) with small holes for hydrogen injection. A hydrogen manifold located outside the burner was connected to the five circular tube-manifolds in each 90° sector by tubing and a flow-control valve. The outer hydrogen manifold was connected to the hydrogen supply by additional lengths of tubing and a main flow-control valve. The burner was located 5.85 meters (230.5 inches) upstream of the engine inlet guide vanes.

Inlet total-pressure distortion was generated by mounting a screen

configuration on a motor driven rotatable-screen assembly (fig. 4) during combined steady-state pressure-temperature distortion tests only. The screen assembly was located approximately one engine diameter or 0.951 meters (37.4 inches) upstream of the engine inlet guide vanes. The screen configuration used was of 180°-extent and 40.2 percent blockage which produced a total-pressure distortion of 10.7 percent.

As in references 2 through 5, an extended bullet nose was installed between the rotable-screen assembly and the engine inlet. This extended bullet nose provided the surface for the installation of a row of hub static taps and hub boundary layer measurements.

Instrumentation

Inlet duct and engine inlet instrumentation is outlined schematically in figures 2 and 5. Pressures were recorded on scanivalves and calibrated for a range of 0 to 69 kPa (10 psia). Temperatures were measured using chromel-alumel thermocouples referenced to a 339K (610°R) oven. Reference 11 discusses Mach number recovery corrections used for thermocouples.

The inlet duct and extended bullet nose wall boundary layer yaw (circumferential variation) probes are detailed in figure 6. Yaw angle is positive when the tangential flow component is in the direction of fan rotation, figure 6. An inlet guide vane pitch-yaw probe is sketched in figure 7. This probe was mounted on the leading edge of an inlet guide vane and measured the freestream pitch (radial) angle in addition to the yaw angle of a streamline. The pitch angle is positive when the radial flow component is oriented from tip to hub (fig. 7). The station 2 pitch-yaw probe is of similar design. With the exception of one temperature rake at 47 degrees, flow angle probes were circumferentially positioned at duct locations which avoided wakes from upstream instrumentation. Probe calibrations were obtained over a flow angle range of $\pm 30°$ at the same stream Mach number conditions as encountered during engine tests. The estimated systematic error is about $\pm 2/3°$, and the random error is roughly $\pm 1/2°$. Additional information on flow angle measurements can be found in reference 12.

PROCEDURE

The hydrogen burner was used to produce steady-state temperature distortion at the engine face. With the burner at the 0° position (see fig. 3), quadrants I and II were ignited and the gaseous-hydrogen flow increased until the average temperature at the engine face (0° to 180° position) was approximately 361K (650°R) and a data point was recorded. Quadrant I of the burner was then shutdown and quadrant III of the burner was ignited and hydrogen flow increased until quadrants II and III produced approximately 361K (650°R) at the engine face (90° to 270° position).

This mode of burner sector operation maintained 180°-extent temperature distortion but rotated the distortion by 90°. This procedure was continued until the 180°-extent temperature distortion was completely rotated over the engine face. A total of 4 steady-state data points were recorded at each burner position of -30°, 0°, +30°. The result is twelve data points per rake for each profile. The same procedure was utilized for 90°-extent temperature distortion tests. The average temperature over the distorted sectors for these tests was approximately 339K (610°R).

The rotation of the temperature distortion for temperature distortion tests was used in conjunction with the rotating screen assembly for the steady-state combined pressure-temperature distortion tests. The burner was set at 0° or rotated ±30° from the zero position. The 180°-extent screen was rotated such that one of the following four configurations pertained: (1) the screen preceded the 180°-extent temperature distortion by 90°, (2) the screen completely overlapped the 180°-extent temperature distortion, (3) the screen lagged the 180°-extent temperature distortion by 90° and (4) the screen was 180° out-of-phase to the 180°-extent temperature distortion. A total of twelve data points in increments of 30° were recorded for each of the 4 hydrogen-burner and screen assembly orientations. The average temperature over the distorted sectors for these tests was approximately 317K (570°R).

For both steady-state temperature distortion and combined pressure-temperature distortion tests the presentation of a set of 12 data points is identical. The burner was set at 0° and the first data point was plotted at its installed angular rake (or tap) position. The second data point was then plotted at a step of 30° but in the opposite direction to burner rotation or index of ignited burner sectors. This procedure is analogous to holding the burner in the fixed position and rotating the instrumentation. Pressure data was corrected to upstream plenum pressures in order to compensate for run-to-run variations.

At each of the inlet duct wall and bullet nose static taps (fig.5), a maximum and minimum static pressure was identified for each distortion test series of 12 data points. The difference between this maximum and minimum was normalized with a similar difference at the static taps nearest the IGV's (station 2B) and presented as a relative static distortion level.

The constant Reynolds Number Index (RNI) was achieved by maintaining approximately a 289K (520°R) total temperature in the undistorted sectors of the burner and adjusting the undistorted inlet total pressure to obtain a value of 0.5 RNI. Low-rotor mechanical speed was adjusted during temperature distortion and combined distortion tests in order that the corrected low-rotor speed based on the undistorted burner sectors resulted in speeds of 6000 and 8600 rpm.

TEMPERATURE DISTORTION RESULTS

Flow Angles

Clean inlet.- In order to obtain the net effects of distortion extent or position on flow angle, the clean inlet (no distortion) flow angles must be subtracted from the temperature and temperature-pressure produced flow angles. Figure 8 shows the undistorted streamline flow angles at the entrance to the inlet guide vanes (IGV's) as a function of corrected low-rotor speed. The pitch (radial) and yaw (circumferential) angles range between +2° to -1° and are relatively constant with change in speed. The flow angle profiles presented in this report have not been corrected for the clean inlet configuration.

Low-rotor speed variation.- Figure 9 shows that a change in low-rotor speed has only a slight effect on flow angle amplitude. Flow angle data obtained at 8600 rpm has a slightly larger amplitude than data obtained at 6000 rpm. A computation using the data presented in curve (F-1), figure 9 reveals that a change in station 2C hub flow angle, $\Delta\beta$, $(\beta_{max}-\beta_{min})$ value measured over the relative circumferential position of the flow measurement probe is 9° for the 8600 rpm data and 7.25° for the 6000 rpm data. The sensitivity of a change in hub flow angle is therefore .058 degrees per percent change in engine speed and .148 degrees per percent change in total-temperature distortion. The slight variation between the two sets of data is therefore due mostly to the difference in total-temperature distortion defined as $(T_{max}-T_{min})/T_{avg}$ and noted in the figure. The maximun, minimum and average values in the above expression refer to rake average values. The low-rotor speeds and the Reynolds Number Index were corrected to the undistorted sectors of station 2 for all the tests.

An examination of figure 9 flow angle profiles reveals that the pitch angle variation is reduced and the yaw angle variation is increased as a streamline approaches the engine inlet. Also at the IGV's (Sta. 2C), the yaw angle variation is larger (+6° to -2.5°) than the pitch angle variation (+2° to 0°). The magnitudes of both pitch and yaw angles (freestream and boundary layer) at the engine inlet is largest in the hub region. These results are similar to those noted in reference 13 for steady-state pressure distortion tests. It should be noted that station 2 boundary layer yaw data presented in figure 9 was obtained with the outer most immersion probes.

Distortion extent.- The effect of temperature distortion extent on flow angles at stations 2C and 2 is shown in figure 10. As in the figure 9 profiles, pitch angle variation decreases and yaw angle variation increases as a streamline approaches the engine inlet. Distortion extent does not effect pitch angle circumferential variation at the tip and midspan regions of the IGV's. Curve (C-1) of figure 10 shows that distortion extent does influence the angular location but not the magnitude of the peak pitch angle in the hub region of the IGV's.

Distortion extent does influence the angular location but not the magnitude of the peak yaw angle. The largest yaw angle variation occurs in the hub region of the engine inlet but there is no noticeable increase in yaw angle between stations 2 and 2C.

Lastly curve (A-3) of figure 10 shows the variation of hub and tip boundary layer yaw angle at station 2. The largest variation in flow angle occurs in the hub region of the engine inlet near the extended bullet nose surface. As in the other profiles of figure 10, distortion extent influences the angular location but not the magnitude of the boundary layer flow angle profile.

There is a slight difference in amplitude between data recorded at an extent of 90° and 180° as observed in figure 10. A computation using data presented in curve (F-1), figure 10 shows a change in station 2C hub flow angle, $\Delta\beta$, $(\beta_{max}-\beta_{min})$ measured over the relative circumferential position of the flow measurement probe to be 5.4° for the 180° extent data and 4.8° for the 90° extent data. The sensitivity of a change in hub flow angle is therefore -.037 degrees per percent change in total-temperature distortion. Since both sets of data were recorded at an engine speed of 8600 rpm the slight variation in the data is due to the difference in total-temperature distortion, $(T_{max}-T_{min})/T_{avg}$ as noted in the figure.

Effect of distortion type.- Figure 11 compares the variation of hub yaw angle data at station 2C (IGV entrance) obtained from steady-state 180°-extent pressure and temperature distortion tests.

The curves in figure 11 show that for both types of distortion low-rotor speed has a slight effect on yaw angle magnitude. The interesting aspect of the figure is that steady-state pressure and temperature distortions produce yaw angle profiles which are 180° out-of-phase with each other. Steady-state 180°-extent pressure distortion produces a yaw-angle profile which varies 31.8° (+16.8° to -15°) with peak positive and negative yaw angles located circumferentially at 13° and 173°. Steady-state 180°-extent temperature distortion produces a yaw angle profile which varies 9.1° (+6.3° to -2.8°) with a peak positive yaw angle at 203° and a peak negative yaw angle at 23°. In both cases the distortion extended from 0° to 180°.

The maximun positive yaw angle produced by pressure distortion occurs as a rotor blade enters a low static pressure region and the maximum negative yaw angle occurs as the rotor blade exits the low static pressure region. Pressure distortion results in a flow into the low pressure region behind the screen. The existence of a low static pressure region from 0° to 180° is verified by the static-pressure profile shown in figure 12. Similarly temperature distortion heats the air over the extent of 0° to 180° causing the air to expand and thus increase the static pressure level as shown in figure 12. The result of the increase in static pressure is flow out of the high temperature region between the burner and engine inlet.

Static-Pressure Distortion

An investigation of static-pressure distortion change along the inlet duct wall and bullet nose extension for variations in low-rotor speed, distortion extent and effect of the type of distortion (temperature or pressure) is shown in figures 13 through 15. The value of static pressue-distortion was obtained by determining the maximum and minimum pressures at each static tap location from the test set of 12 data points (see Procedure). The distortion change presented in this report is the same as that used in reference 13 and defined as (Ps,max-Ps,min) for each location, normalized by ($Ps_{,max}$-$Ps_{,min}$) at station 2B, or, $\Delta Ps/(\Delta Ps)2B$. The total-temperature distortion in percent is defined and noted for data presented in figures 13 through 15. The total-pressure distortion in percent is defined and noted in figure 15.

Presentation of inlet-duct wall data.- The duct wall data of figure 13(A) compares more favorably with the exponential curve of reference 10 than the bullet nose data of figure 13(B). From the duct wall data of figure 13(A) it is observed that the 8600 rpm data matches the exponential curve for values of (x/r_m) over the range of 0.18 to 1.

From figures 14 and 15 it is observed that 180°-extent temperature distortion with a total-temperature distortion range of 18.7 to 31.3 percent results in static pressure profiles which compare favorably with the exponential curve over the range $(x/r_m) \leq 1$.

Temperature and Pressure Profiles

Axial variation of temperature and pressure along inlet duct.- Figure 16 describes the axial variation of freestream rake-average total temperatures at station 1 (downstream of the burner) and station 2 (upstream of the engine inlet). The total-temperature profiles show that there is no change in total-temperature level with axial distance. The data in figure 16(A) is at a slightly higher amplitude than the data of figure 16(B) due to a higher total-temperature distortion value as noted in the figure.

Figure 17 shows total and static-pressure profiles at the inlet to the IGV's. The solid line in figure 17(B) shows a predicted static-pressure profile using Mazzawy's model (ref.3). Although the model prediction is for the IGV inlet, it is compared to stations 2B and B (two static tap measurements closest to the IGV's) as static pressure measurements are not available at the IGV inlet. It is noted from the figure that the model satisfactorily predicts pressure levels.

COMBINED DISTORTION RESULTS

Flow Angles

The effect of combined pressure-temperature distortion on freestream and boundary layer yaw angles at stations 2C and 2 are shown in figure 18. Streamline pitch angle variation is not discussed since the pitch angle at station 2C is small in magnitude when compared to yaw angle.

Yaw angle variation.- An examination of figure 18 indicates that yaw angle amplitude increases as the streamline approaches the engine inlet. The largest yaw angle variation also takes place in the hub region of the engine inlet. The latter statement applies to both freestream and boundary layer regimes. These results are similar to those obtained during steady-state temperature and pressure distortion tests. The largest variation in both freestream and boundary layer yaw angle at stations 2C and 2 occurs when the pressure-temperature distortions are 180° out-of-phase. This result is expected if we consider the yaw angle profile associated with pressure or temperature distortion as presented schematically in figure 19(A) and 19(B). Over a 180°-extent distortion, the yaw angle slope is negative for pressure distortion and positive for temperature distortion. For combined distortion with pressure and temperature distortions 180° out-of-phase with each other the resultant yaw angle variation is larger than the yaw angle variation associated with other combined distortion orientations as the yaw angle profiles for each individual distortion (temperature and pressure) are aligned (180° out-of-phase, see fig. 19(C)). The smallest variation in both freestream and boundary layer yaw angle at stations 2C and 2 occurs when pressure-temperature distortions overlap (superimposed). For this combined distortion orientation the yaw angle profile associated with each individual distortion is opposed resulting in a reduction in profile amplitude as shown in figure 19(D).

It should be noted from figure 18 that the maximum and minimum yaw angles are not exactly at the edges of the pressure distortion but are within the distorted sector of the flow field. This indicates that the extent of the low pressure field produced by the screen is slightly less than the intended 180°. Also at these edge points a probable error in yaw angle measurement of approximately 1° occurs because of the steep total-pressure gradients. This error is in addition to that mentioned in the Instrumentation section. A correction would decrease the yaw angle magnitude shown at these locations.

Change in inlet yaw angle.- Figure 20 shows the variation in hub region yaw angle, $\Delta\beta$, $(\beta_{max} - \beta_{min})$ with static-pressure distortion at Sta. 2B (static tap location nearest the IGV's). As static pressure distortion at the engine inlet increases, the streamline at the edge of the distortion entering the engine is turned through a correspondingly

larger yaw angle. The apparent generalization of the flow angle variation shown on figure 20 indicates that it is a function of static pressure distortion rather than total pressure and total temperature, separately or in combination. At the hub section shown, the sensitivity is approximately 3 degrees per percent of static pressure distortion. Pressure distortion data shown in this plot was obtained from reference 13.

Static Pressure Distortion

Figure 21 shows the static-pressure distortion change along the inlet duct wall and bullet nose extension for variations in pressure and temperature distortion orientation.

The exponential curve of reference 10 satisfactorily predicts static pressure amplification in the range of $(x/r_m) \leq 1$. Flow in the region of $(x/r_m) > 1$ is complex and the exponential prediction does not adequately predict static-pressure amplitude. The static-pressure distortion results along the inlet duct wall and extended bullet nose surface, are similar to steady-state temperature distortion tests previously discussed and the steady-state pressure distortion tests presented in reference 13.

Temperature and Pressure Profiles

Axial variation of temperature and pressure profiles along the inlet duct.- Figure 22 describes the axial variation of freestream rake-average total pressures and total temperatures between Station A (downstream of the screen) and station 1 (downstream of the hydrogen burner) to the engine inlet. The pressure and temperature profiles show that there is no change in total-pressure and total-temperature amplitude with axial distance as flow approaches the engine inlet. The data also shows the relationship of the pressure and temperature profiles to each other based on the orientation of each distortion device (screen and hydrogen burner). When the two distortion devices are 180° out-of-phase with each other each half of the engine inlet is subjected to only one type of distortion. This orientation produces the total-temperature and total-pressure profiles shown in figure 22(A). When the 180°-extent distortion patterns produced by the screen and the hydrogen burner are superimposed on each other one half of the engine inlet is subjected to both distortions. The total-temperature and total-pressure profiles associated with this configuration are shown in figure 22(C). Inlet total-pressure and total-temperature data for the two 90° overlapping distortion orientations are shown in figure 22(B) and 22(D).

Static pressure profiles at engine inlet.- Static-pressure profiles at station 2B (nearest to the engine inlet) for different orientations of combined pressure and temperature distortion are shown in figure 23. The sinusoidal profiles and the distortion orientation diagrams shown

on the figure verify that streamlines at the engine inlet enter a low static-pressure region from 0° to 180°, produced by a 180°-extent screen. Pressure distortion results in a flow into the regions behind the screen. Similarly an increase in amplitude of static-pressure profiles from 180° to 360° is due to 180°-extent temperature distortion. Temperature distortion heats the air causing air to expand over the 180°-extent and therefore the corresponding increase in static-pressure profiles.

An examination of the sinusoidal profiles of figure 23 shows that from 0° to 90° the lowest static pressure level occurs for the orientations where: 1) pressure distortion precedes temperature distortion by 90° and 2) pressure and temperature distortion are 180° out-of-phase. These two distortion orientations result in pressure distortion only over the first 90° sector. From 90° to 270° the profile which has the steepest positive gradient is for the distortion orientation where pressure distortion leads temperature distortion by 90°. This orientation has a 180°-extent temperature distortion from 90° to 270° which results in expansion of heated air and the resultant increase in profile gradient. The sector which extends from 270° to 360° shows that distortion orientations where: 1) temperature distortion is 180° out-of-phase with pressure distortion and temperature distortion precedes pressure distortion by 90° results in profiles which produce the highest static pressure level due to the temperature distortion in this quadrant.

Figure 24 compares the variation in static-pressure profiles at the engine inlet produced by combined pressure-temperature distortion with that predicted using Mazzawy's model (ref. 3). The model prediction as previously noted is for the IGV inlet but is compared to station 2B data as static pressure measurements are not available at the IGV inlet. It is observed from the figure that the model satisfactorily predicts static pressure level between 30° to 330°. The model does not adequately predict sinusoidal pressure level from 0° to 30° (the first 30° of pressure distortion) and from 330° to 360° (the last 30° of the undistorted region). A more thorough comparison of combined pressure-temperature distortion data with Mazzawy's model is presented in ref. 14.

SUMMARY OF RESULTS

A TF30-P-3 turbofan engine fitted with an extended bullet nose was tested with steady-state inlet circumferential temperature distortion and combined pressure-temperature distortion. The results in terms of inlet flow angle, static-pressure distortion and circumferential temperature and pressure profiles are summarized as follows:

1. Pitch angle (radial variation) is much smaller than yaw angle (circumferential variation) for both temperature distortion and combined distortion.
2. Yaw angle variation is usually largest in the hub region for

the temperature levels and screen configuration tested. Yaw angle variation increases in magnitude as flow approaches the engine inlet.

3. Station 2 boundary layer yaw angle was largest in the hub region for both temperature distortion and combined distortion tests.

4. Yaw angle data obtained from inlet circumferential temperature distortion tests resulted in flow angle profiles which were 180° out-of-phase with flow angle profiles obtained from inlet circumferential combined pressure-temperature distortion tests.

5. An increase in extent from 90° to 180° for inlet circumferential temperature distortion tests had no effect on pitch or yaw angle magnitude.

6. Temperature-induced and combined temperature and screen-induced static-pressure distortions increased exponentially as flow approached the engine inlet.

7. Temperature-induced total temperature circumferential profiles remain nearly constant as flow approaches the engine inlet.

8. Combined temperature and screen-induced total-pressure and total-temperature profiles remain nearly constant as flow approaches the engine inlet.

9. The static-pressure distortion profiles at the engine inlet are sinusoidal for all combined distortion orientations tested.

10. The sensitivity of a change in hub region yaw angle is approximately 3 degrees per precent of static pressure distortion. This statement is valid for steady-state pressure, temperature and combined distortion at the engine inlet.

APPENDIX - SYMBOLS

e	natural Logarithm base
IGV	inlet guide vane
N1	low-rotor speed, rpm
$N1R2_{UD}$	low-rotor speed corrected to undistorted sectors at station 2, $N1/\sqrt{\theta_2}$, rpm
P	pressure, Pa
RNI_{UD}	Reynolds Number Index based on values measured in the undistorted sectors of inlet, $\delta/(\mu/\mu_{SLS}) \cdot \sqrt{\theta}$
r_m	mean radius of IGV, 0.34m
T	Temperature, K
U	tangential velocity, m/sec
V_a	axial velocity, m/sec
x	length, m
Δ	maximum-minimum value
α	pitch angle, deg.
β	yaw angle, deg.
δ	ratio of total pressure to standard sea-level static pressure
Θ	ratio of total temperature to standard sea-level static temperature
μ	absolute viscosity, kg/(m-sec)

Subscripts:

A	station A, pressure measurement station located 83.55cm upstream of inlet guide vanes
AVG	average
B	station B, row of static taps along inlet duct wall and extended bullet nose
MAX	maximum value
MIN	minimum value

S static condition

SLS standard sea-level static condition

T total condition

1 station 1, airflow metering station, located 250.24cm upstream of inlet guide vanes

2 station 2, engine inlet temperature and flow angle measurement, located 13.39cm upstream of the inlet guide vanes

2A station 2A, engine inlet pressure measurement, located 44.41cm upstream of inlet guide vanes.

2B station 2B, start of static pressure taps along inlet duct wall and extended bullet nose, located 6.17cm upstream of inlet guide vanes

2C station 2C, flow angle measurement at entrance to inlet guide vanes

REFERENCES

1. Mazzawy, R. S.: Multiple Segment Parallel Compressor Model for Circumferential Flow Distortion. J. Eng. Power, vol. 99, no. 2, Apr. 1977, pp. 288-296.

2. Mazzawy, R. S.; and Banks, G. A.: Modeling and Analysis of the TF30-P-3 Compressor System with Inlet Pressure Distortion. (PWA-5302, Pratt & Whitney Aircraft; NASA Contract NAS3-18535). NASA CR-134996, 1976.

3. Mazzawy, R. S.; and Banks, G. A.: Circumferential Distortion Modeling of the TF30-P-3 Compression System. (PWA-5448, Pratt & Whitney Aircraft; NASA Contract NAS3-18535). NASA CR-135124, 1977.

4. Evans, D. G.; et al.: Some Comparisons of the Flow Characteristics of a Turbofan Compressor System with and without Inlet Pressure Distortion. NASA TM X-71574, 1974.

5. de Bogdan, C. E.; et al.: Effect of a 180° Extent Inlet Pressure Distortion on the Internal Flow Conditions of a TF30-P-3 Engine. NASA TM X-3267, 1975.

6. de Bogdan, C. E.; Moss, J. E., Jr.; and Braithwaite, W. M.. Internal Flow Characteristics of a Multistage Compressor with Inlet Pressure Distortion. NASA TM X-3446, 1977.

7. Braithwaite, W. M.. Experimental Evaluation of a TF30-P-3 Turbofan Engine in an Altitude Facility: Effect of Steady-State Temperature Distortion. NASA TM X-2921, 1973.

8. Rudey, R. A.; and Antl, R. J.: The Effect of Inlet Temperature Distortion on the Performance of a Turbofan Engine Compressor System. AIAA Paper 70-625, 1970.

9. Abdelwahab, Mahmood: Effect of Temperature Transients at Fan Inlet of a Turbofan Engine. NASA TP-1031, 1977.

10. Plourde, G. A.; and Stenning, A. H.: Attenuation of Circumferential Inlet Distortion in Multistage Axial Compressors. J. Aircr., vol. 5, no. 3, May-June 1968, pp. 236-242.

11. Glawe, George E.; Simmons, Frederick S.; and Stickney, Truman M.: Radiation and Recovery Corrections and Time Constants of Several Chromel-Alumel Thermocouple Probes in High Temperature, High Velocity Gas Streams. NACA TN-3766, 1956.

12. Dudzinski, T. J.; and Krause, L. N.: Flow-Direction Measurement with Fixed-Position Probes. NASA TM X-1904, 1969.

13. Soeder, Ronald H.; and Bobula, George A.: Effect of Steady-State Pressure Distortion on Flow Characteristics Entering a Turbofan Engine. NASA TM-79134, 1979.

14. Braithwaite, W. M.; and Soeder, Ronald H.: Combined Pressure and Temperature Distortion Effects on Internal Flow of a Turbofan Engine. NASA TM-79136, 1979.

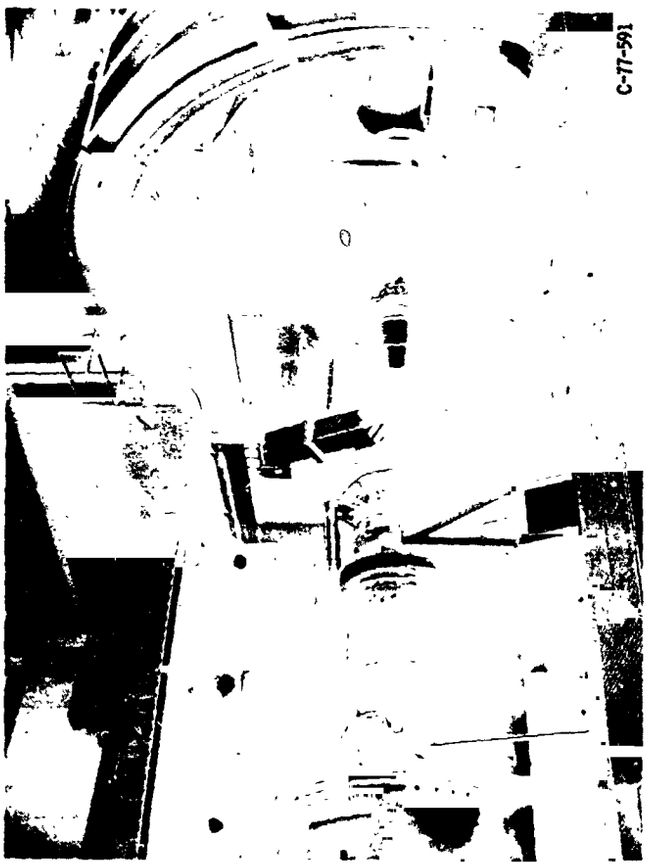

Figure 1. - TF30-P-3 engine in altitude test chamber.

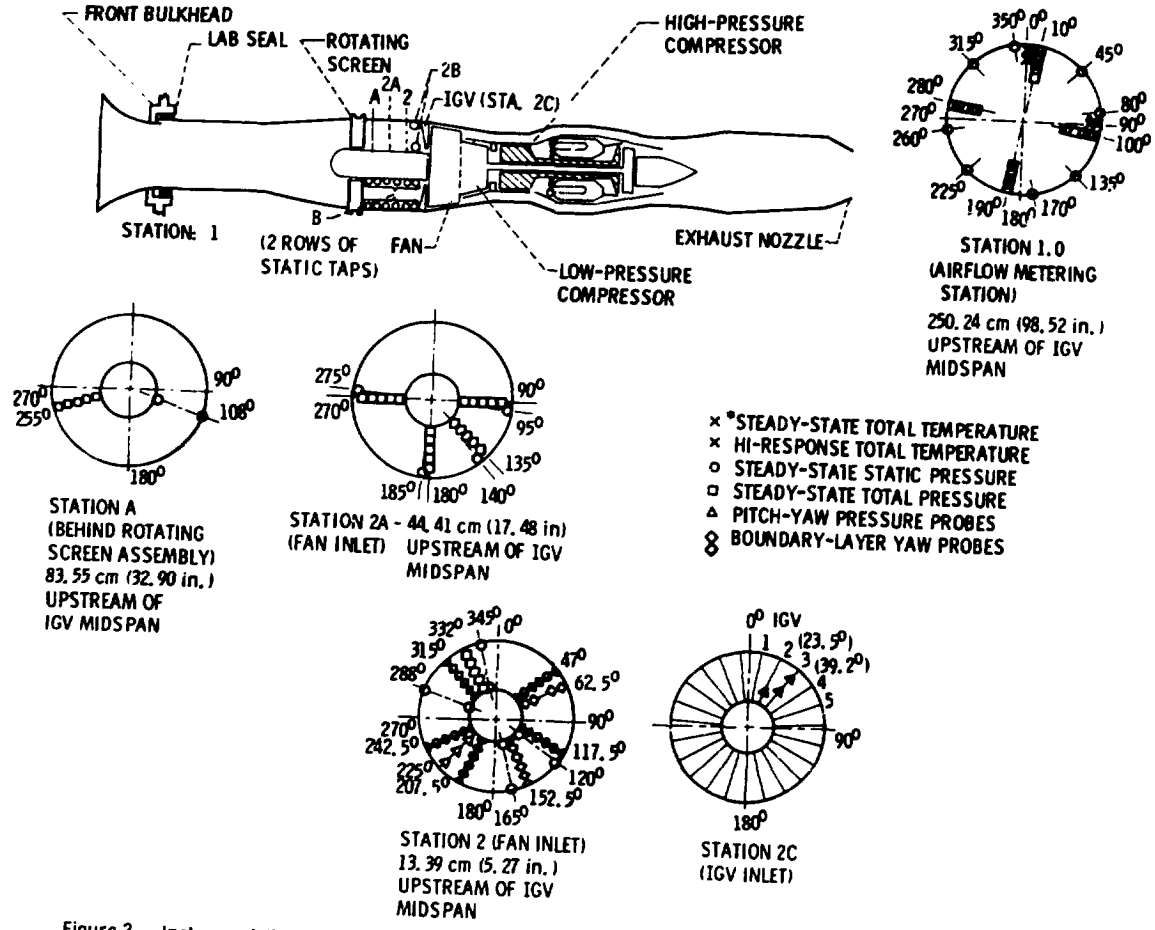

Figure 2. - Instrumentation layout for TF30-P-3 turbofan engine. (Instrumentation stations viewed looking upstream.)

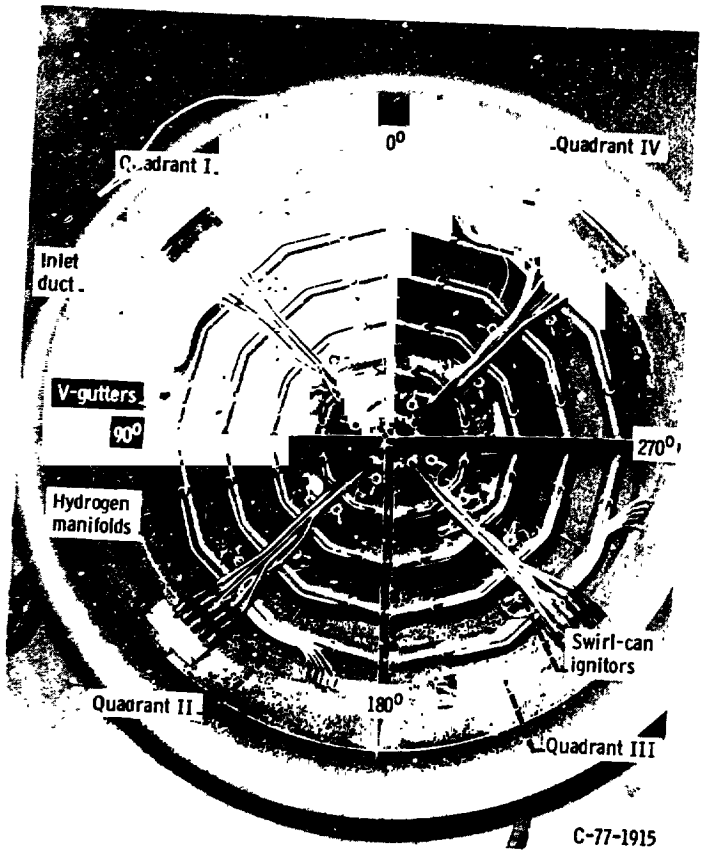

Figure 3. - Gaseous-hydrogen-fueled burner viewed in the direction of engine inlet.

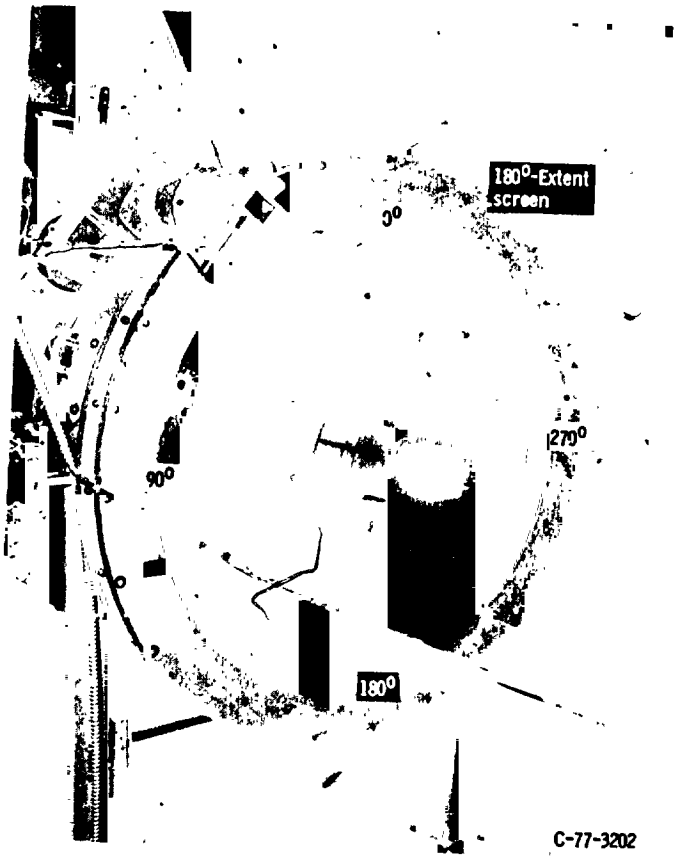

Figure 4. - Rotating screen assembly, viewed in the direction of the engine inlet.

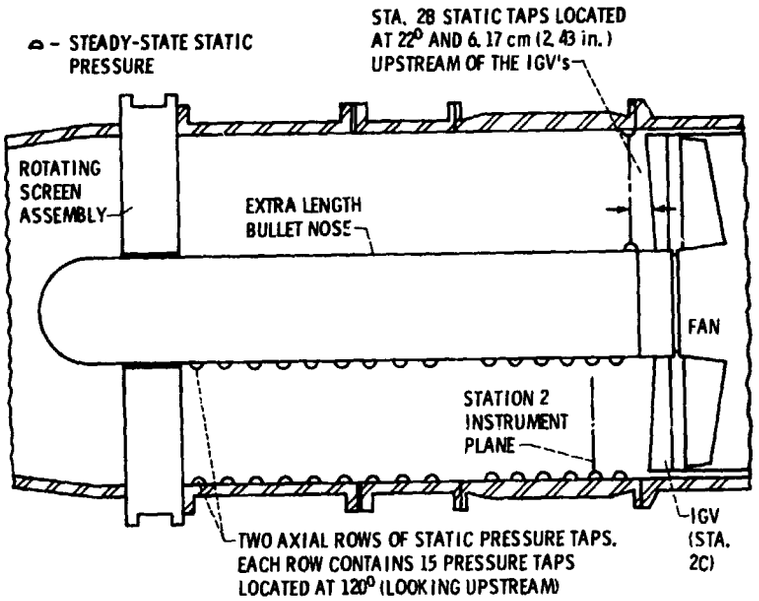

Figure 5. - Bullet nose extension, Station B.

PROBE	D	E	NO. REQUIRED
TIP	0.51 cm (0.20 in.)	1.02 cm (0.40 in.)	1
HUB	0.38 cm (0.15 in.)	0.64 cm (0.25 in.)	1

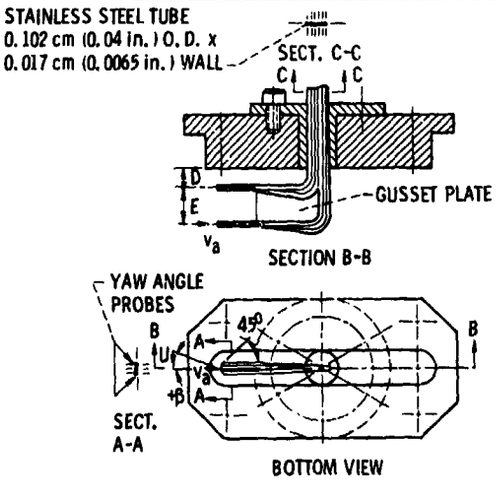

Figure 6. - Tip and hub boundary layer yaw probes located at Station 2 and at 5.1 cm (2 in.) upstream of Station 2.

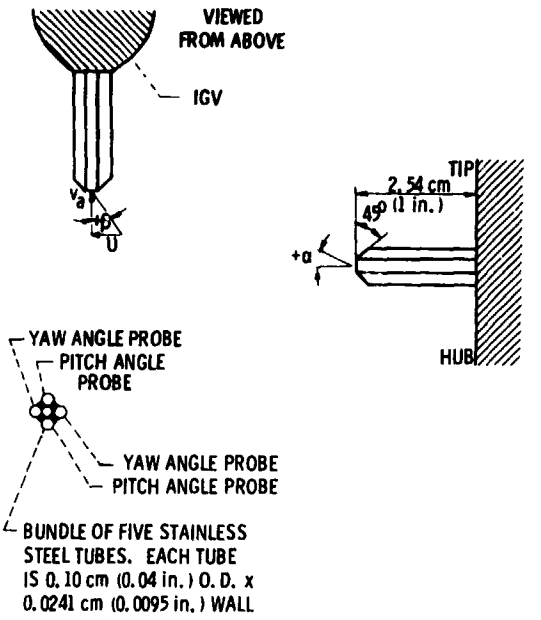

Figure 7. - Sketch of pitch-yaw pressure measurement probes located at station 2C.

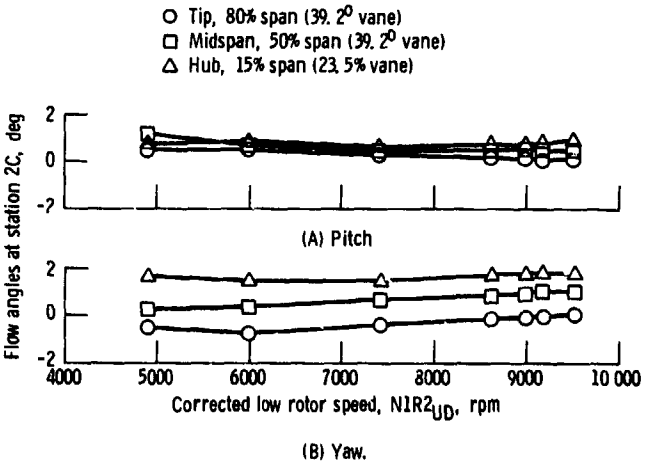

Figure 8. - Flow angles at station 2C (inlet to IGV's) versus low-rotor speed with no temperature or pressure distortion (clean inlet). 0.5 RNI_{UD}.

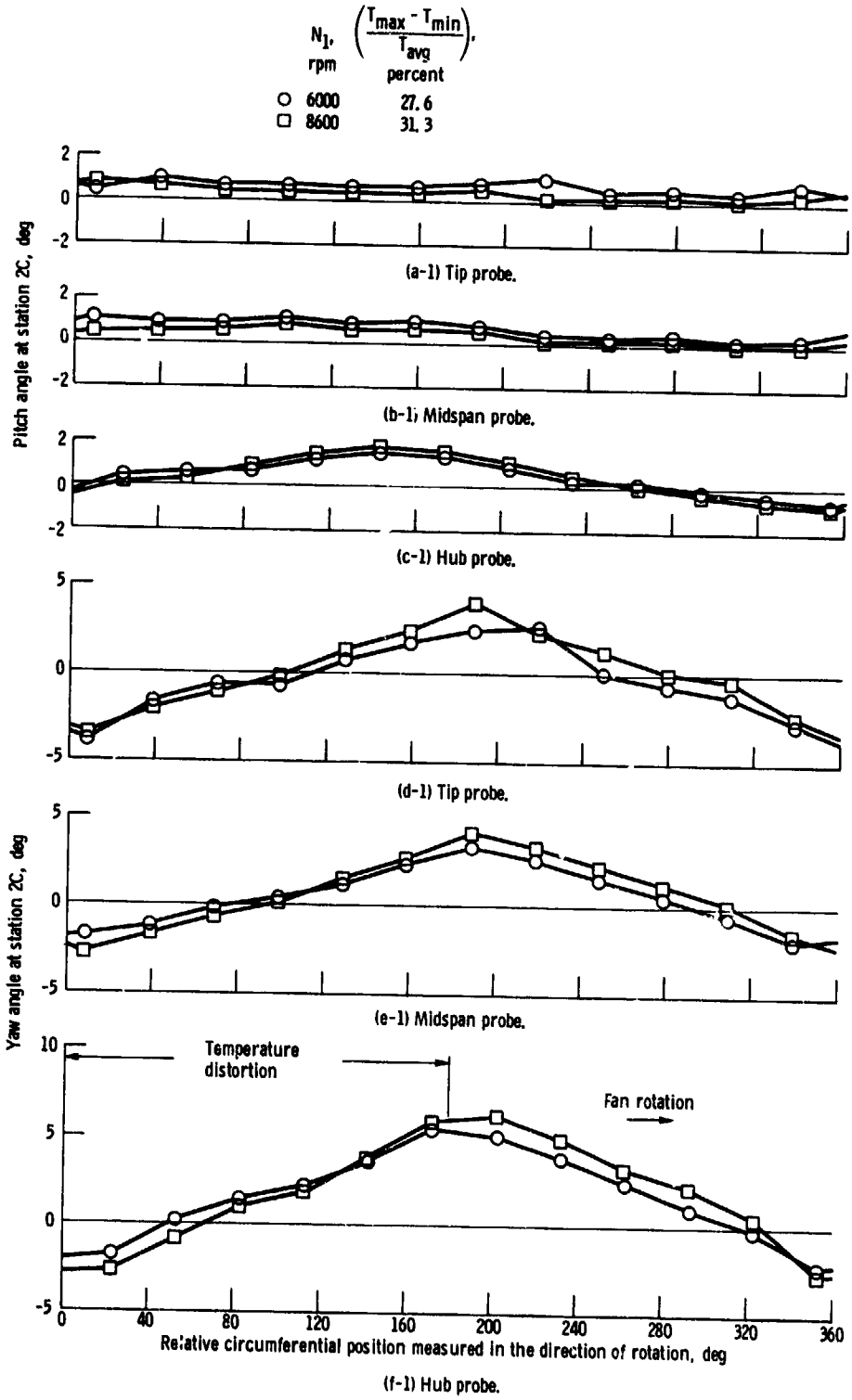

Figure 9. - Effect of low-rotor speed on flow angle variation at station 2C and 2. 180°-extent temperature distortion with heated quadrants at 361 K (650° R) and 0.5 RNI_{UD} based on undistorted pressure and temperature at station 2.

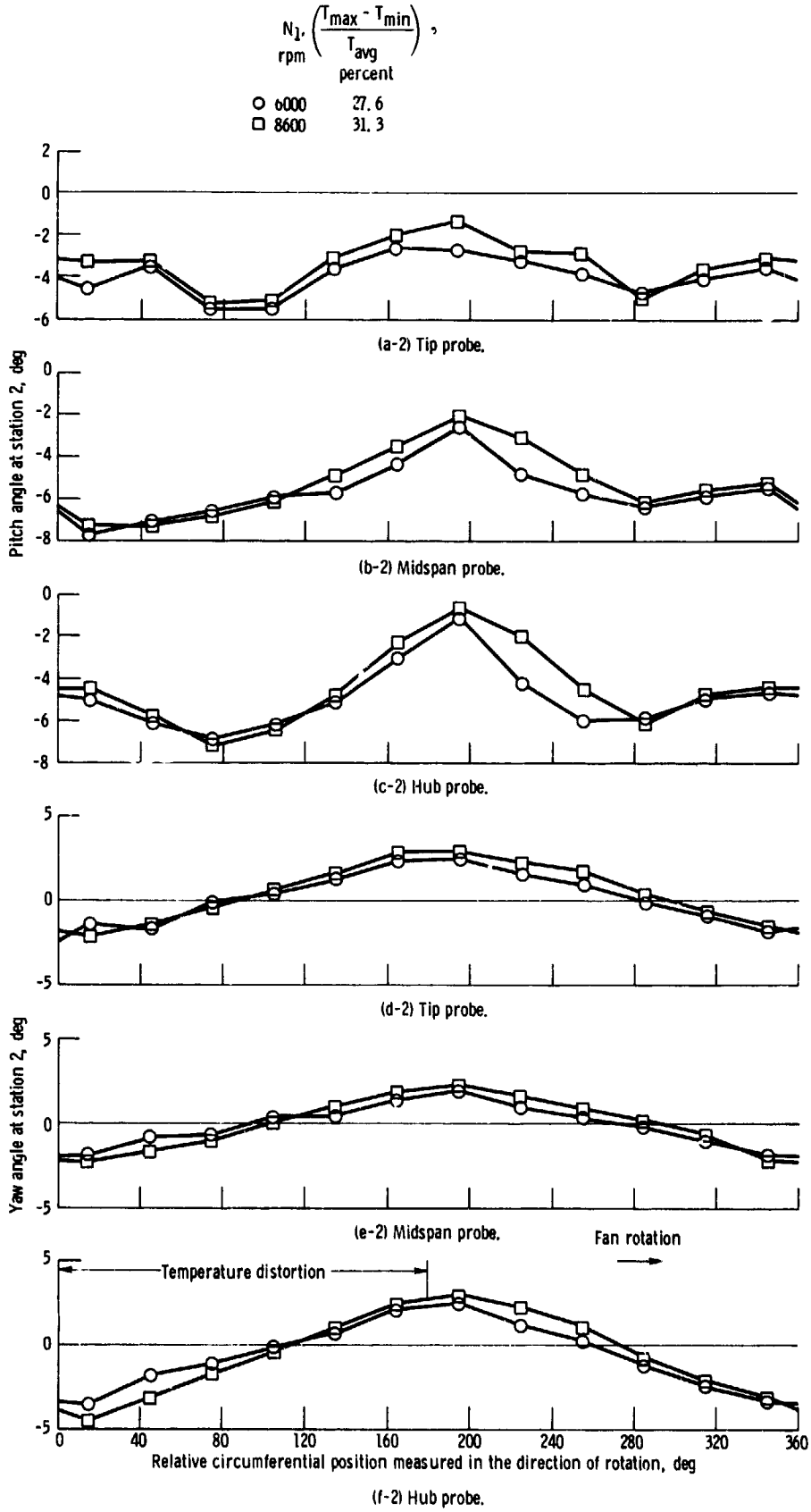

(a-2) Tip probe.

(b-2) Midspan probe.

(c-2) Hub probe.

(d-2) Tip probe.

(e-2) Midspan probe.

(f-2) Hub probe.

Figure 9. - Continued.

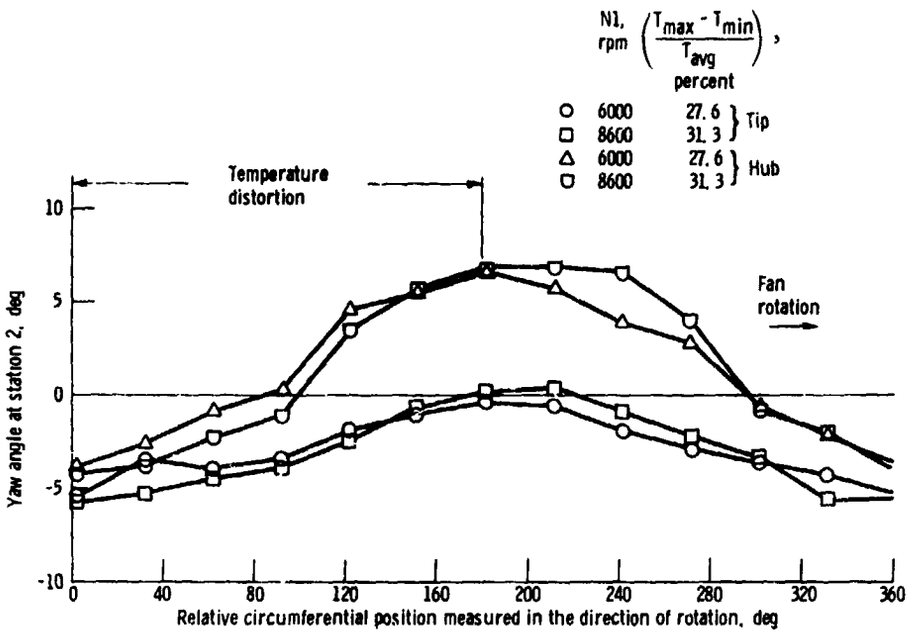

(a-3) Hub-to-tip boundary layer probes.

Figure 9. - Concluded.

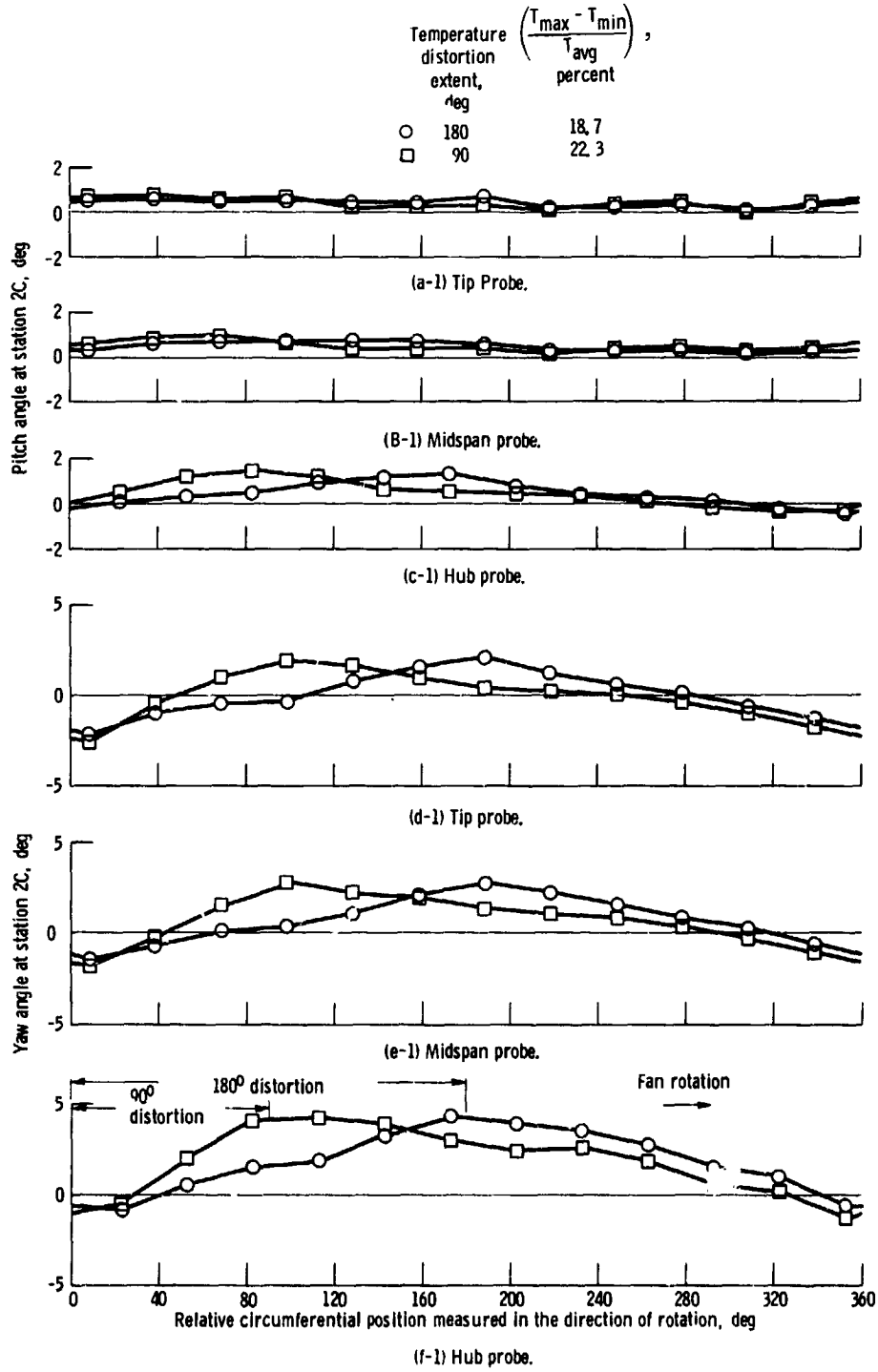

Figure 10. - Effect of temperature distortion extent on flow angle variation at station 2C and 2. Heated quadrants at 339 K (610° R). 8630 rpm low-rotor speed and 0.5 RNI_{UD} based on undistorted pressure and temperature at station 2.

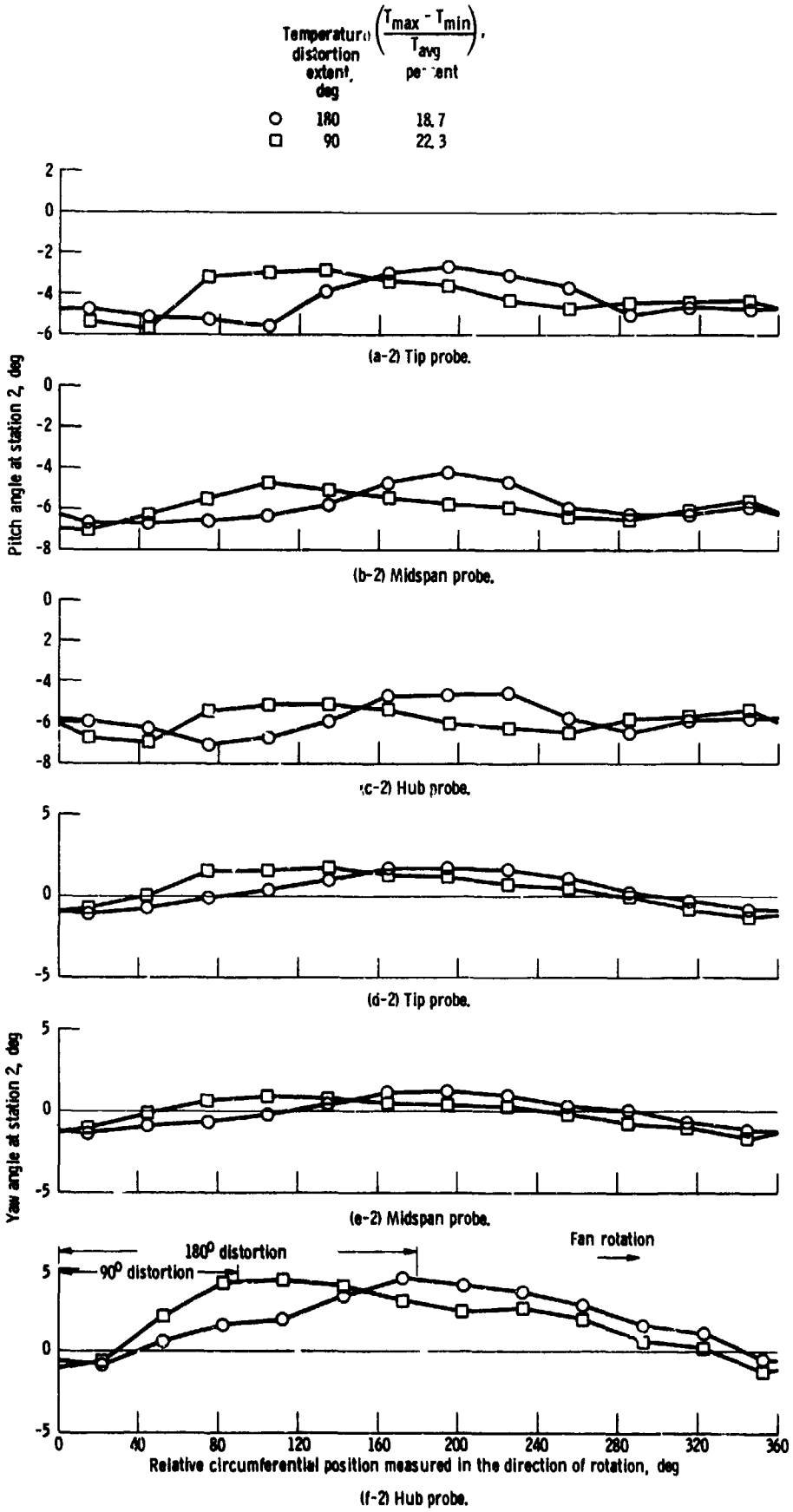

Figure 10. - Continued.

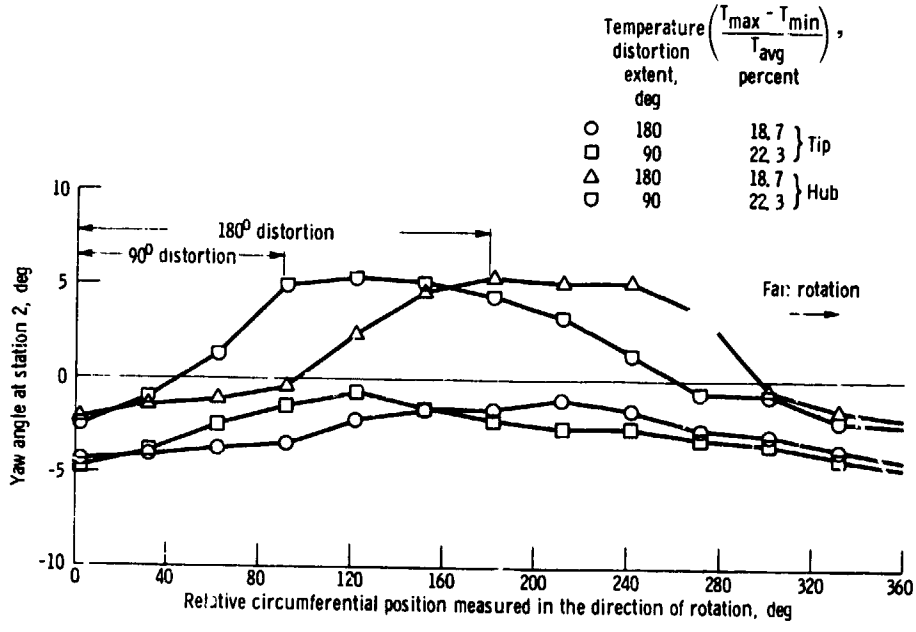

(a-3) Hub-to-tip boundary layer probes.

Figure 10. - Concluded.

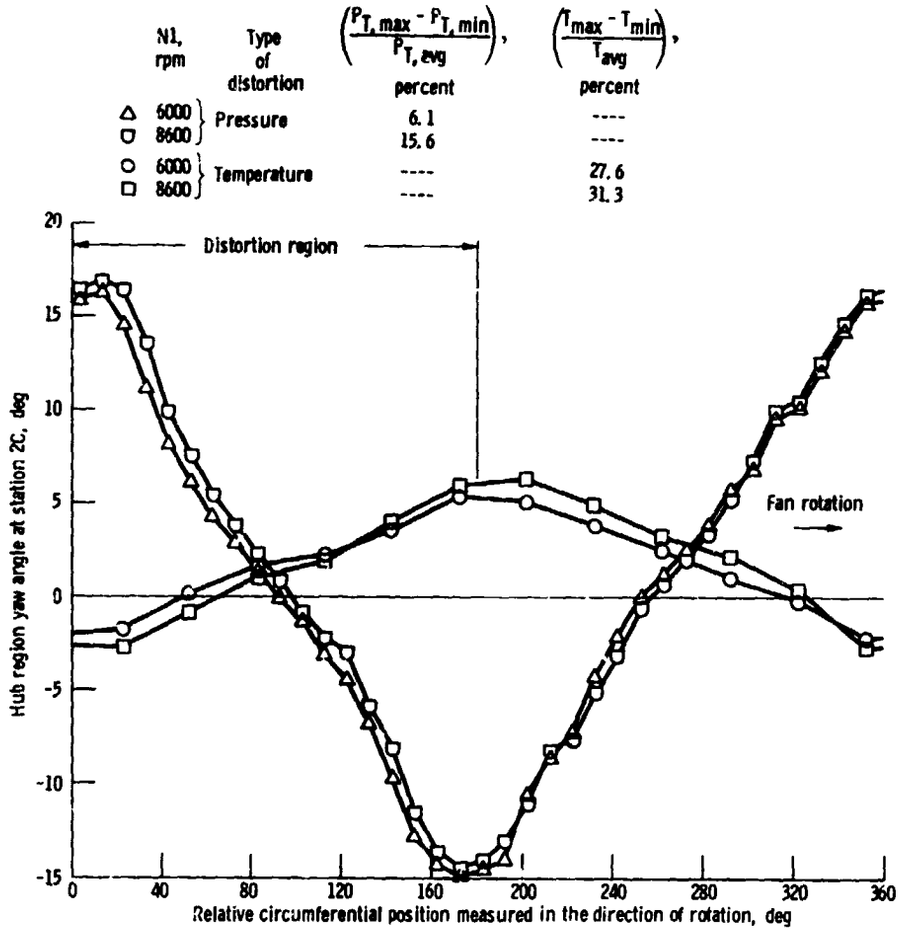

Figure 11. - Hub yaw angle variation at station 2C for 180°-extent pressure distortion using 49.4 percent blockage screen and 180°-extent temp. distortion with heated quadrants at 361 K (650° R). 0.5 RNI_{UD} based on undistorted sectors at station 2.

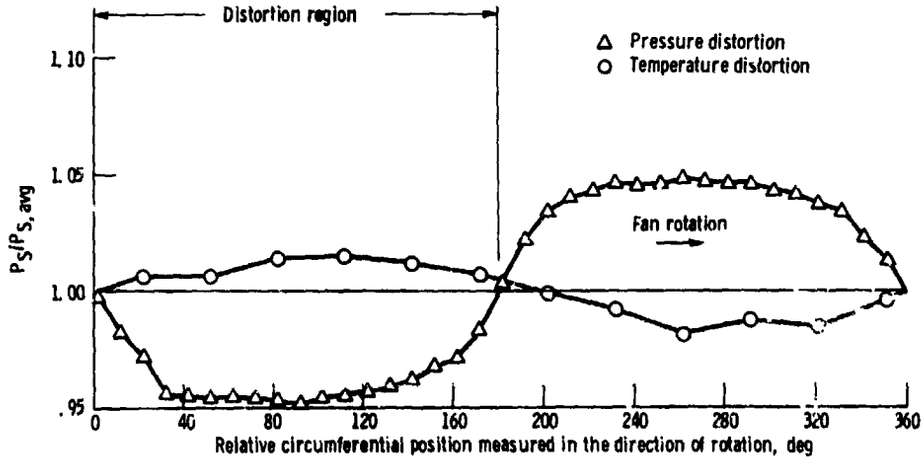

Figure 12. - Circumferential variation of static pressure at station 2B (duct wall) with 15.6 percent total pressure distortion and 31.3 percent total-temperature distortion. 8600 rpm low-rotor speed and 0.5 RNI_{UD} based on undistorted sectors at station 2.

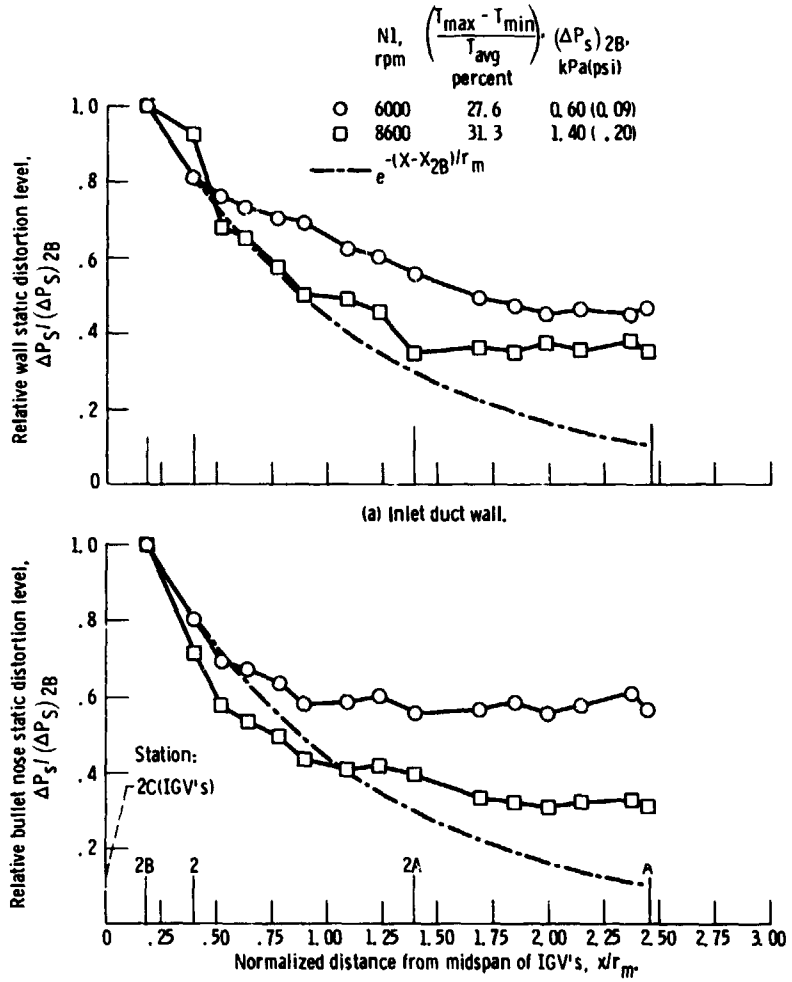

Figure 13. - Effect of low-rotor speed on static-pressure distortion for 180°-extent temperature distortion with heated quadrants at 361 K (650° R). 0.5 RNI_{UD} based on undistorted sectors at station 2.

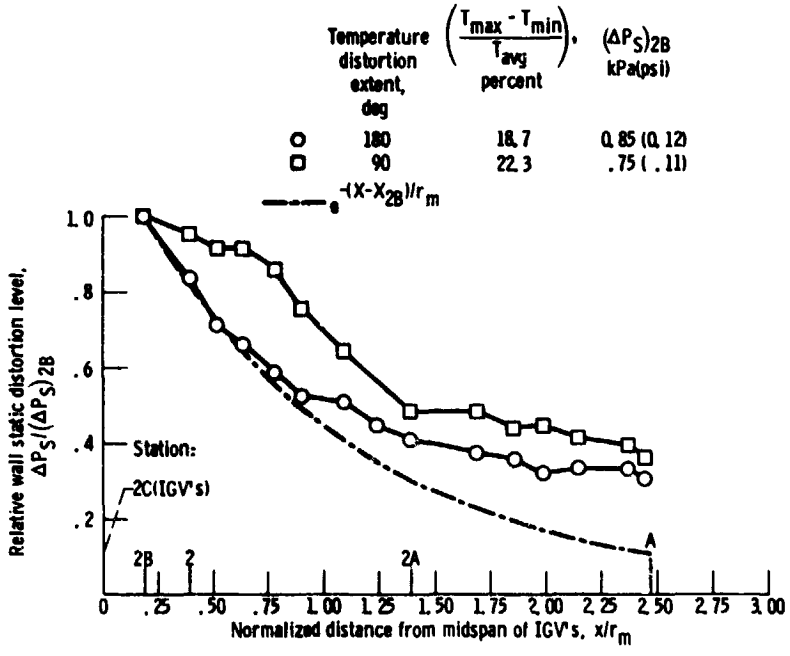

Figure 14. - Effect of temperature distortion extent on static pressure distortion along inlet duct wall. 180°-extent temperature distortion with heated quadrants at 339 K (610° R). 8600 rpm low-rotor speed and 0.5 RNI_{UD} based on undistorted sectors at station 2.

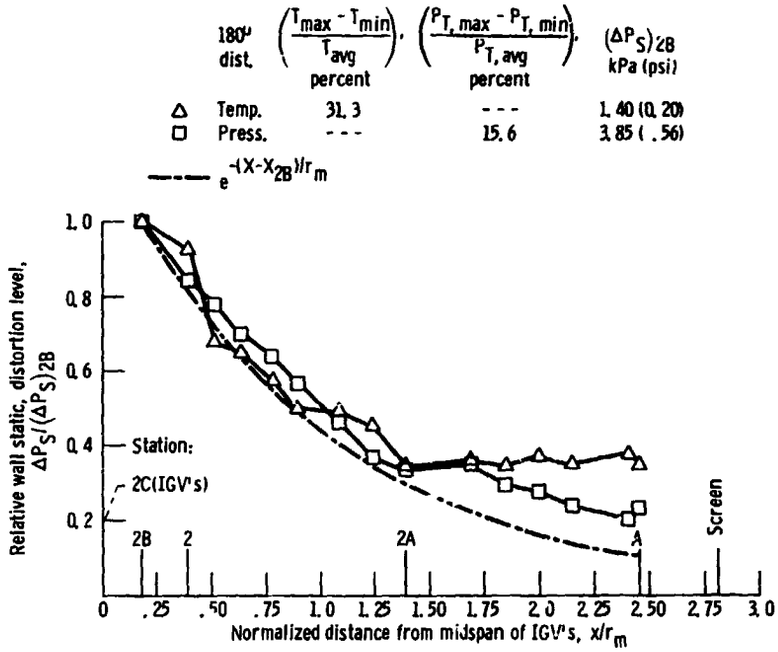

Figure 15. - Effect of 180°-extent, pressure and temperature distortion on static-pressure distortion along inlet duct wall. Pressure distortion produced by 49.4 percent blockage screen and temperature distortion produced by burner with heated quadrants at 361 K (650° R). 8630 rpm low-rotor speed and 0.5 RNI_{UD} based on undistorted sectors at station 2.

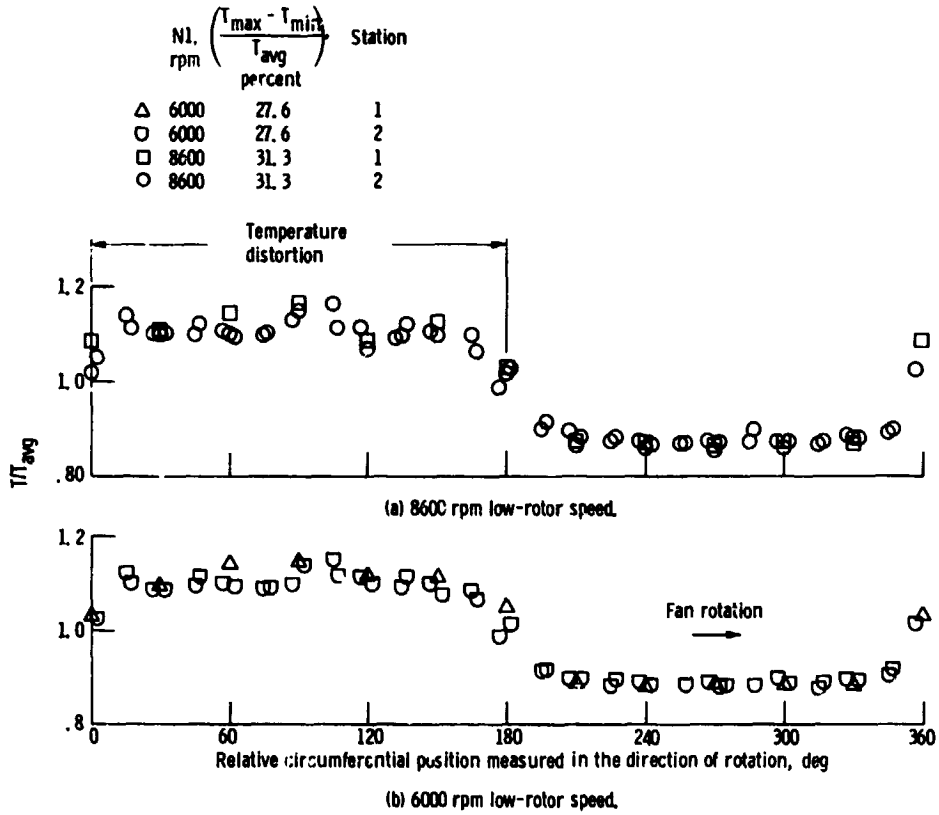

Figure 16. - Circumferential total-temperature variation for 180°-extent temperature distortion with heated quadrants at 361 K (650° R). 0.5 RNI_{UD} based on undistorted sectors at station 2.

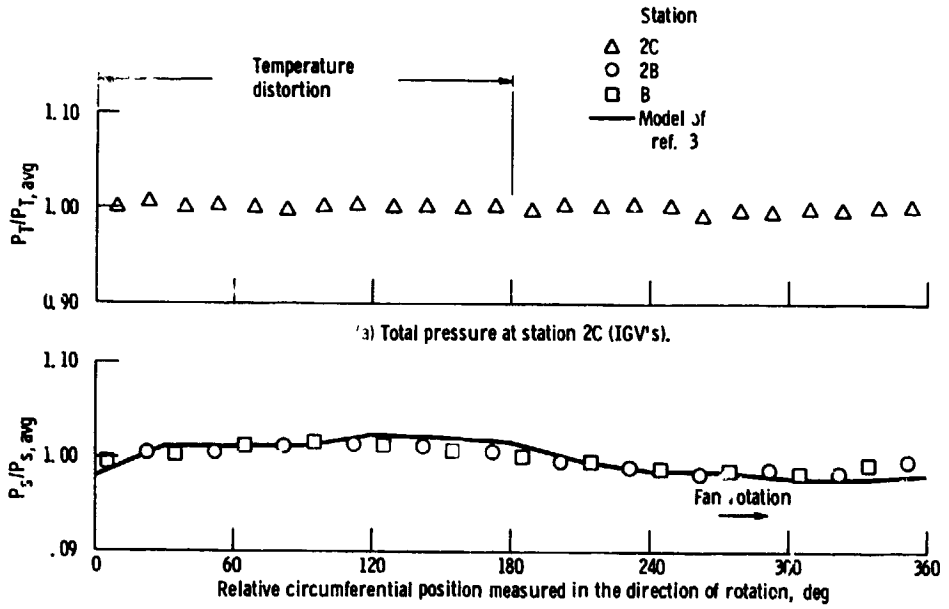

Figure 17. - Circumferential variation of total and static pressure for 180^0-extent temperature distortion with heated quadrants at 364 K (655^0 R). 8600 rpm low-rotor speed and 0 5 RNI_{UD} are based on undistorted sectors at station 2.

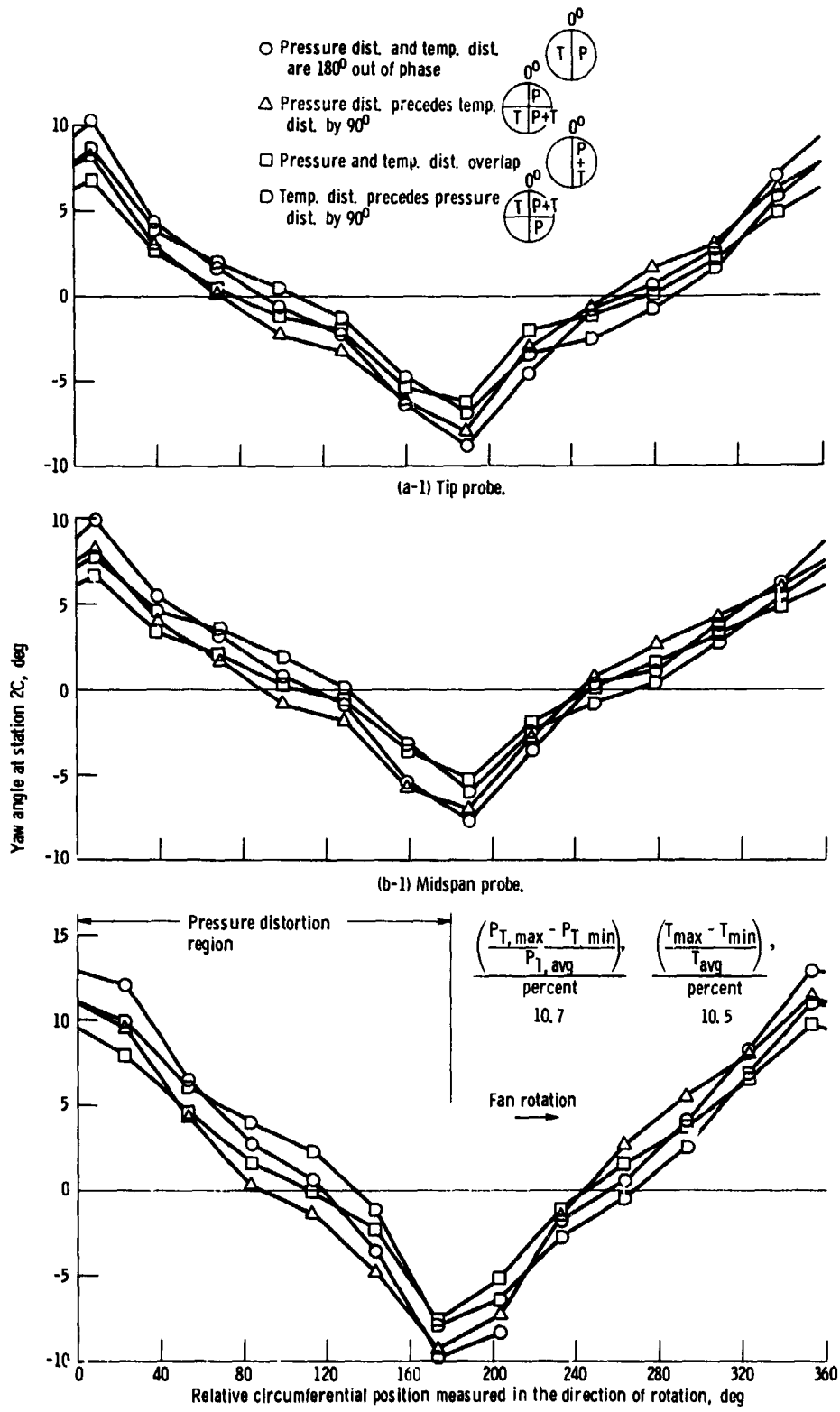

Figure 18. - Effect of combined temperature and pressure distortion on yaw angle variation at station 2C and 2. Pressure distortion produced by 180°-extent, 40.2 percent blockage screen. 180°-extent temperature distortion produced by burner with distorted sectors at engine face at 317 K (570° R), 8600 rpm low-rotor speed and 0.5 RNI_{UD} based on undistorted sectors at station 2.

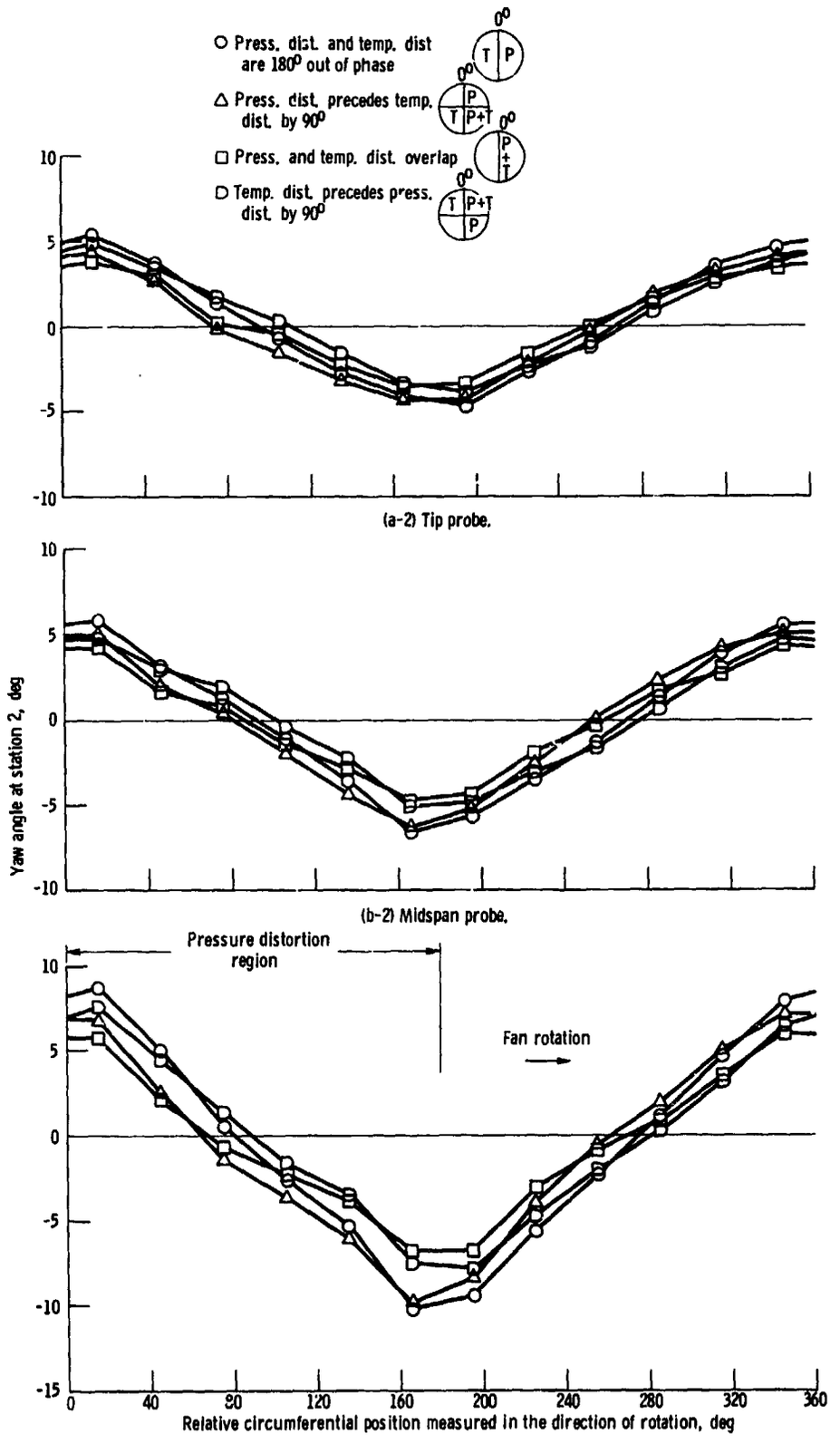

(a-2) Tip probe.

(b-2) Midspan probe.

(c-2) Hub probe.

Figure 18. - Continued.

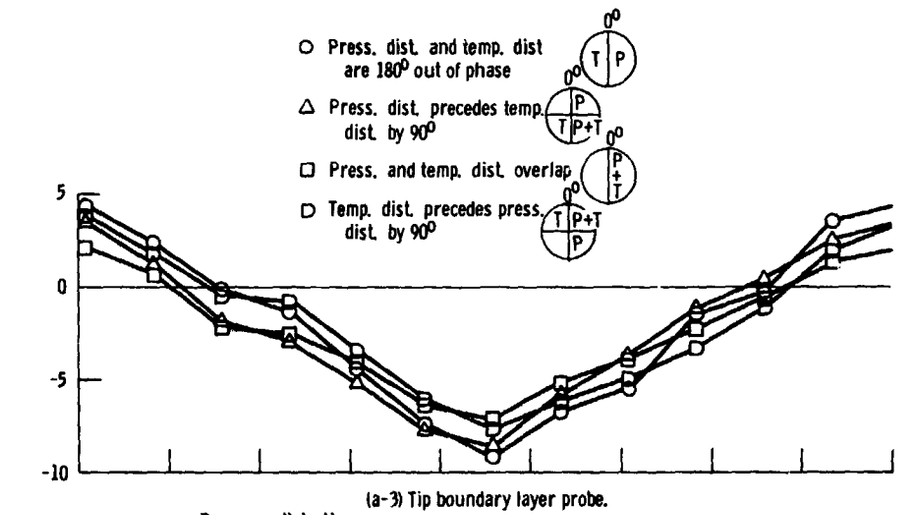

(a-3) Tip boundary layer probe.

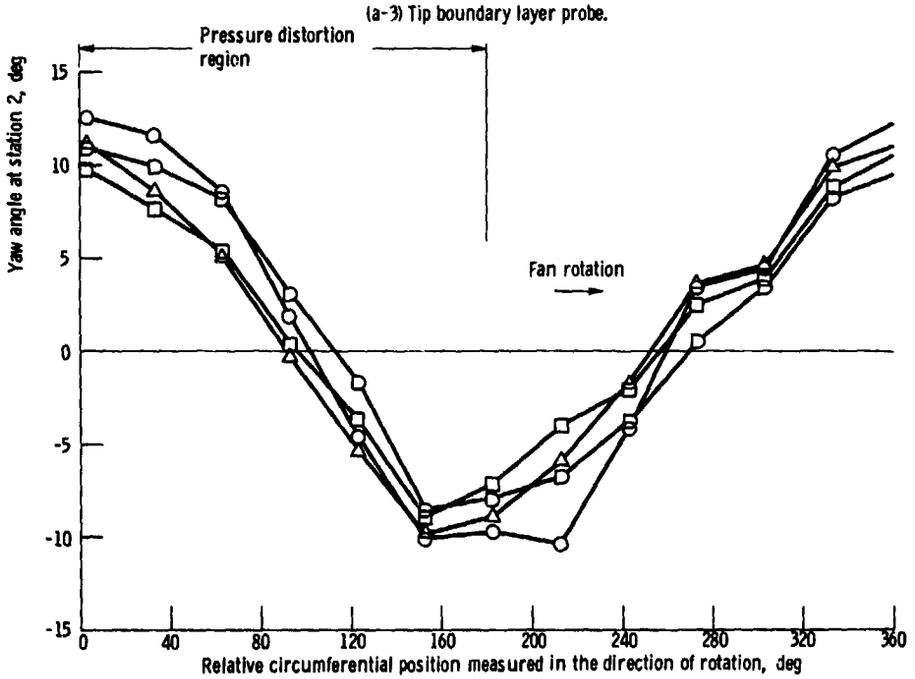

(b-3) Hub boundary layer probe.

Figure 18. - Concluded.

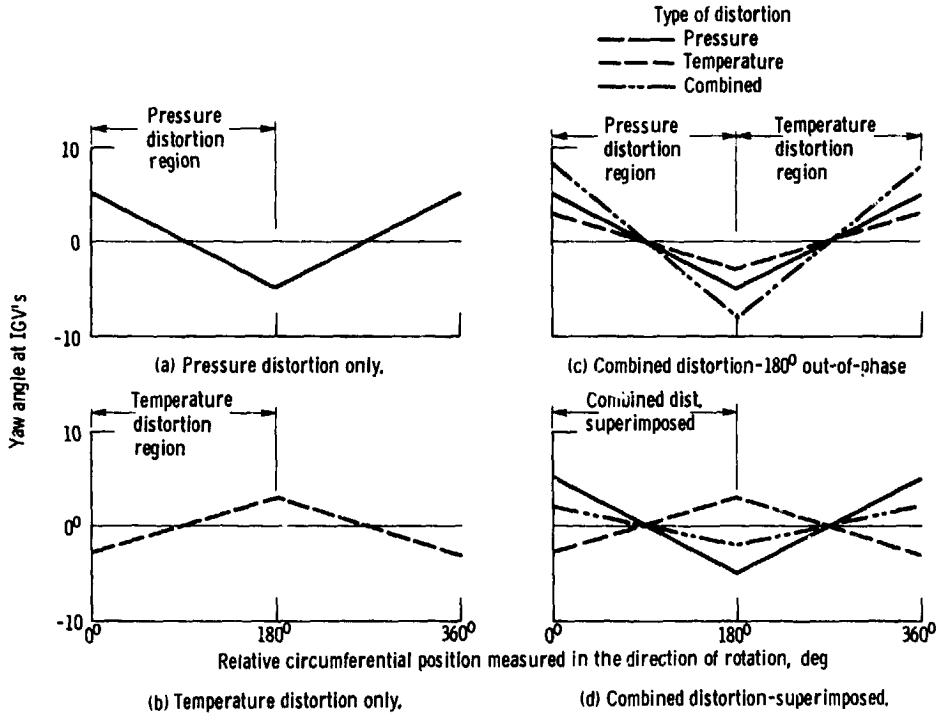

Figure 19. - Schematic presentation of yaw angle variation at engine inlet for pressure, temperature, and combined distortion.

Pressure distortion $\left(\frac{P_{T,max} - P_{T,min}}{P_{T,avg}}\right)$, percent	RNI	Temperature distortion $\left(\frac{T_{max} - T_{min}}{T_{avg}}\right)$, percent	RNI	Combined distortion $\left(\frac{P_{T,max} - P_{T,min}}{P_{T,avg}}\right)$, percent	$\left(\frac{T_{max} - T_{min}}{T_{avg}}\right)$, percent	RNI
15.6	0.5	31.3	0.5	10.7	10.5	0.5
10.2	.5	18.7	.5			
10.2	.35	22.3 (90^0 extent)	.5			
7	.20					

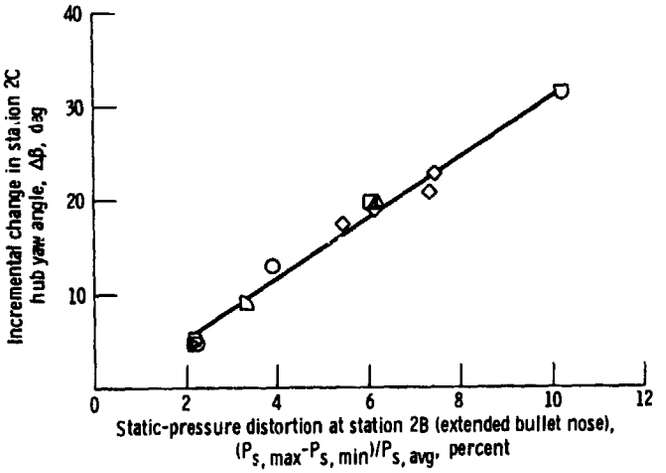

Figure 20. - Change in station 2C hub region yaw angle as a function of distortion level. Distortion extent is 180^0, 8600 rpm low-rotor speed and 0.5 RNI_{UD} based on undistorted sectors at station 2.

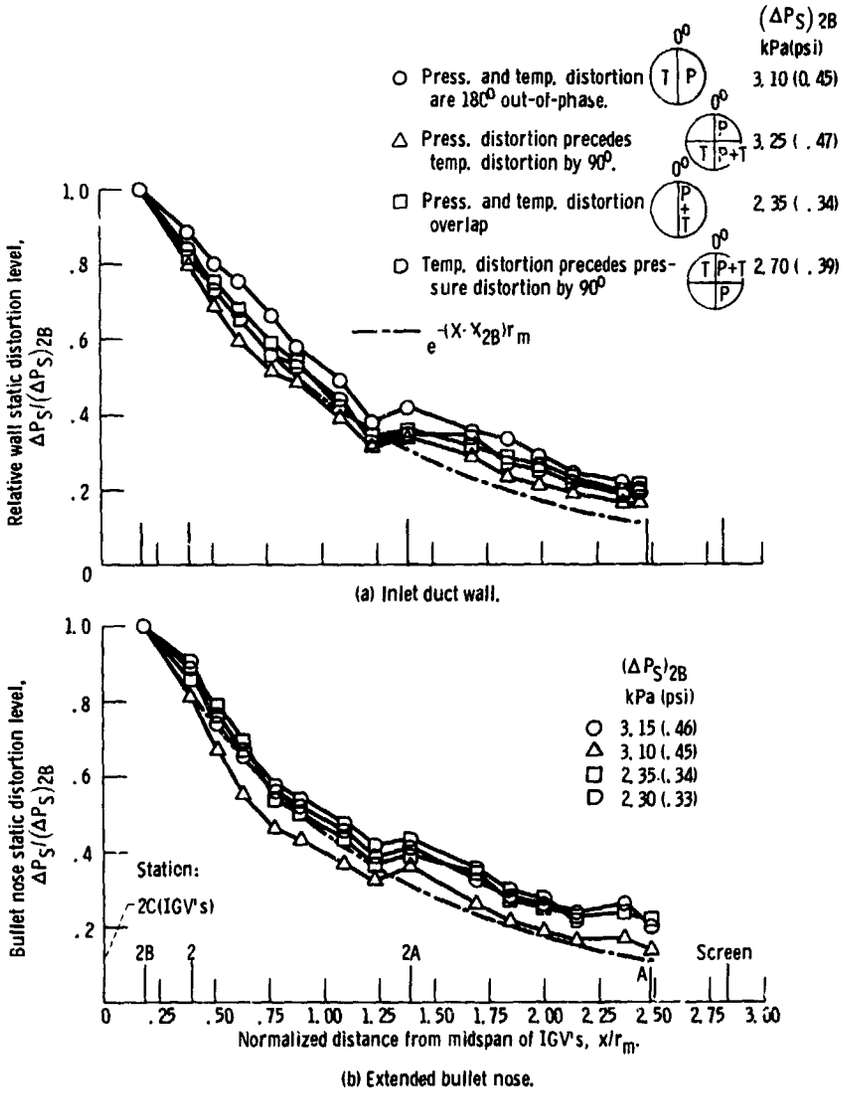

Figure 21. - Effect of pressure and temperature distortion orientation on static-pressure distortion. Pressure distortion produced by 180°-extent, 40.2 percent blockage screen. 180°-extent temperature distortion produced by burner with heated quadrants at 317 K (570° R). 8600 rpm low-rotor speed and 0.5 RNI_{UD} are based on undistorted sectors at station 2.

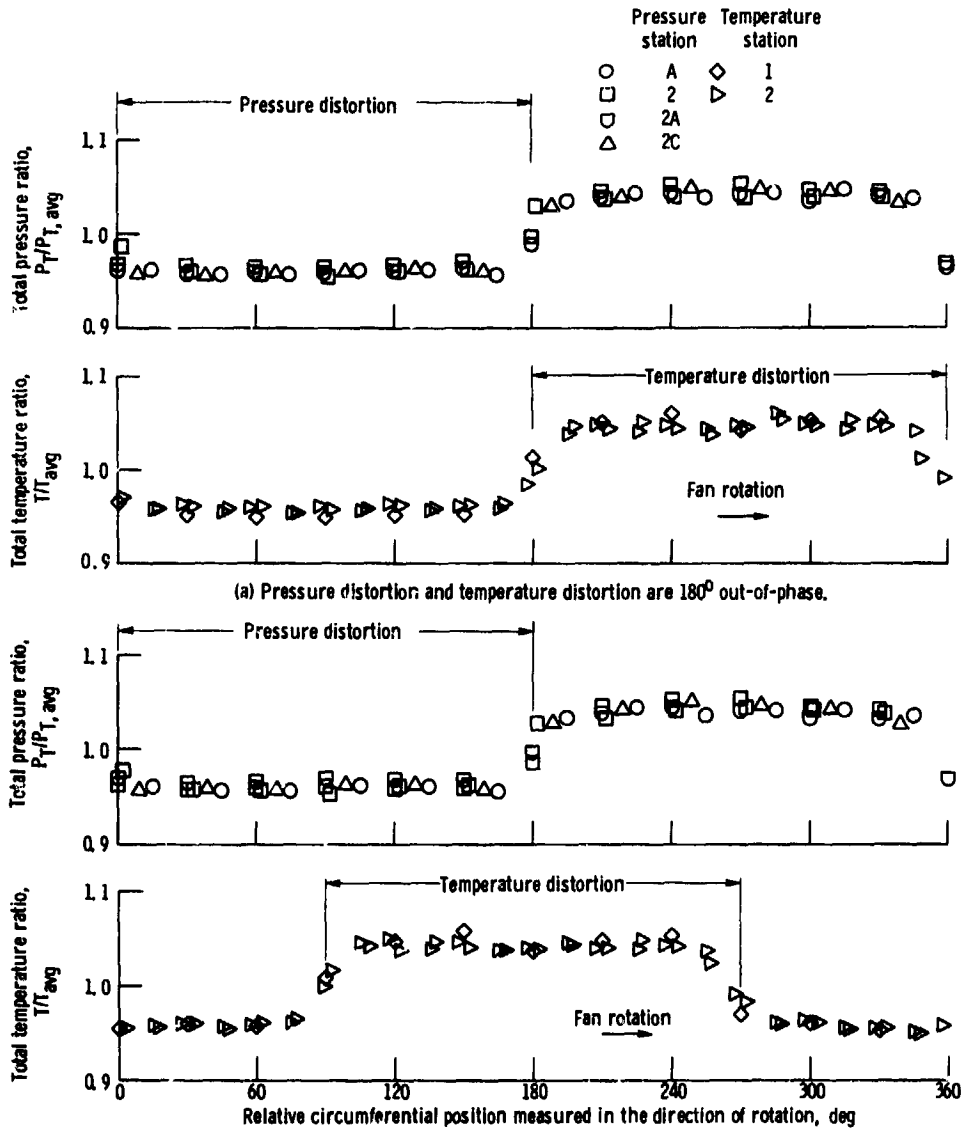

(a) Pressure distortion and temperature distortion are 180° out-of-phase.

(b) Pressure distortion precedes temperature distortion by 90°.

Figure 22. - Circumferential variation of total pressure and total temperature profiles. Distortions produced by 180°-extent, 40.2 percent blockage screen and hydrogen burner with heated quadrants at 317 K (570° R), 8600 rpm low-rotor speed and 0.5 RNI_{UD} are based on undistorted sectors at station 2.

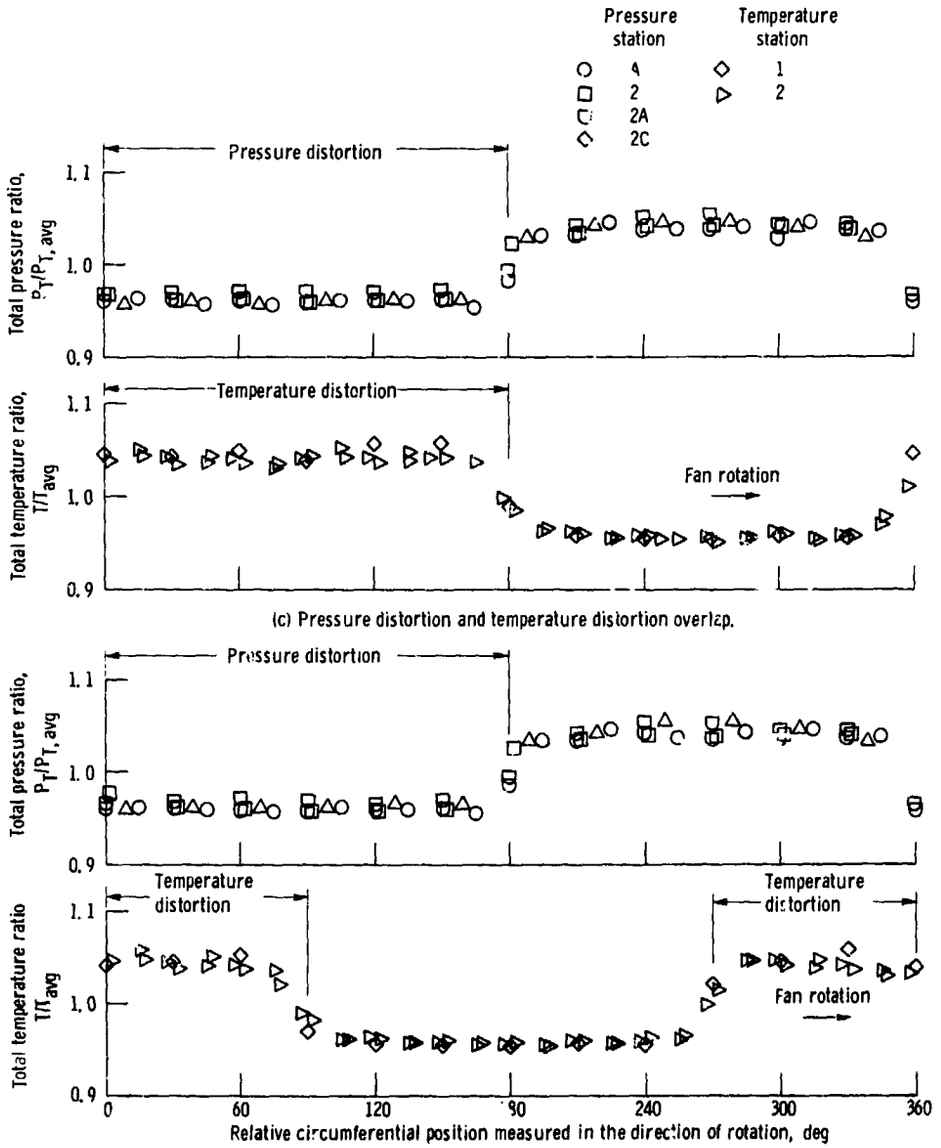

(c) Pressure distortion and temperature distortion overlap.

(d) Pressure distortion lags temperature distortion by 90°.

Figure 22. - Concluded.

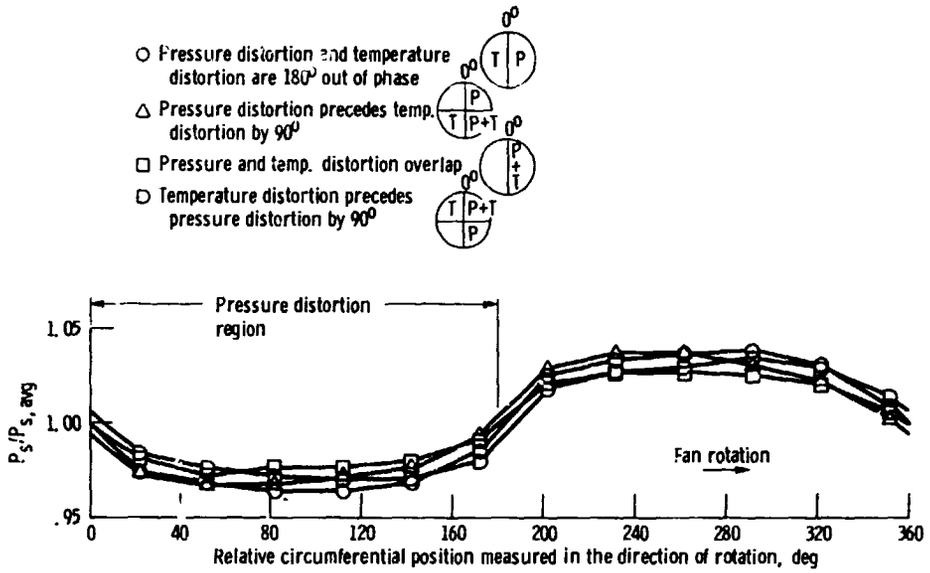

Figure 23. - Circumferential variation of static pressure at station 2B (duct wall). 180°-extent pressure distortion using 40.2 percent blockage screen and 180°-extent temperature distortion produced by burner with distorted sectors at engine face at 317 K (570° R). 8600 rpm low-rotor speed and 0.5 RNI_{UD} are based on undistorted sectors at station 2.

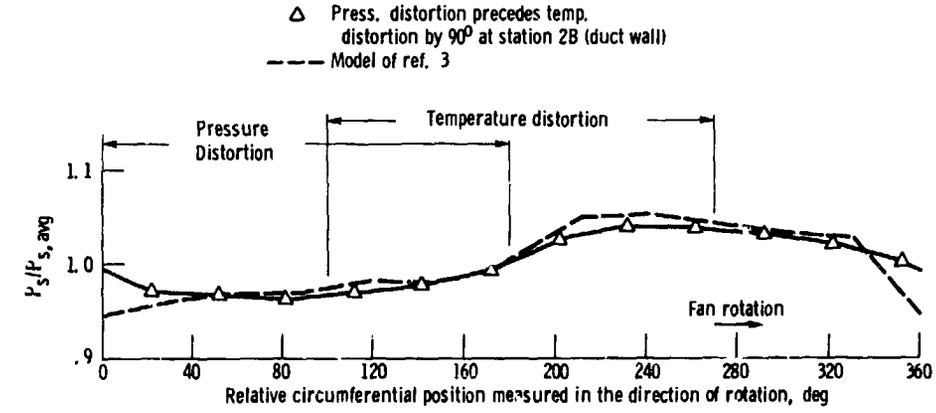

Figure 24. - Circumferential variation of static pressure at engine inlet. Pressure distortion produced by 180°-extent, 40.2 percent blockage screen. 180°-extent temperature distortion produced by burner with distorted sectors at engine face at 317 K (570° R). 8600 rpm low-rotor speed and 0.5 RNI_{UD} are based on undistorted sectors at station 2.